



**HAL**  
open science

# EBP-GEXIT Charts for M-ary AWGN Channel for Generalized LDPC and Turbo Codes

Arti Yardi, Tarik Benaddi, Charly Poulliat, Iryna Andriyanova

► **To cite this version:**

Arti Yardi, Tarik Benaddi, Charly Poulliat, Iryna Andriyanova. EBP-GEXIT Charts for M-ary AWGN Channel for Generalized LDPC and Turbo Codes. *IEEE Transactions on Communications*, 2022, 70 (6), pp.3613-3626. 10.1109/TCOMM.2022.3167027 . hal-03654020

**HAL Id: hal-03654020**

**<https://hal.science/hal-03654020>**

Submitted on 28 Apr 2022

**HAL** is a multi-disciplinary open access archive for the deposit and dissemination of scientific research documents, whether they are published or not. The documents may come from teaching and research institutions in France or abroad, or from public or private research centers.

L'archive ouverte pluridisciplinaire **HAL**, est destinée au dépôt et à la diffusion de documents scientifiques de niveau recherche, publiés ou non, émanant des établissements d'enseignement et de recherche français ou étrangers, des laboratoires publics ou privés.

# EBP-GEXIT Charts for M-ary AWGN Channel for Generalized LDPC and Turbo Codes

Arti Yardi, IIIT-Hyderabad, arti.yardi@iiit.ac.in

Tarik Benaddi, IMT Atlantique, tarik.benaddi@imt-atlantique.fr

Charly Poulliat, IRIT/INPT-ENSEEIH, charly.poulliat@enseeiht.fr

Iryna Andriyanova, ETIS/ENSEA,UCP, CNRS, iryna.andriyanova@ensea.fr

**Abstract**—The maximum a posteriori (MAP) threshold corresponds to the fundamental limit that one can hope to achieve with the given channel code ensemble. Apart from theoretical interests, finding this limit is also desirable since spatial-coupled code ensembles approach this MAP threshold due to phenomenon termed as *threshold saturation*. However finding this MAP threshold, in general, is known to be computationally prohibitive. This work proposes a tractable method for estimating the MAP threshold for various families of sparse-graph code ensembles over non-binary complex-input additive white Gaussian noise (AWGN) channel. Towards this, we provide a method to approximate the extended belief propagation generalized extrinsic information transfer (EBP-GEXIT) chart and estimate the MAP threshold by applying the *Maxwell construction* to it. To illustrate the validity of our method, we study spatial coupling for serially-concatenated turbo-codes and numerically observe threshold saturation of these codes to the MAP thresholds estimated via our method.

**Index Terms**—EBP-GEXIT charts, Maxwell construction, MAP threshold, Spatially-coupled codes, Threshold saturation, Generalized and doubly-generalized LDPC codes, Serially concatenated turbo codes

## I. INTRODUCTION

For a given channel code ensemble, there are three fundamental limits on the channel parameter above which reliable communication is not possible; Shannon threshold, MAP threshold, and belief-propagation (BP) threshold. While Shannon threshold (limit due to channel capacity) is associated with any arbitrary rate  $R$  code ensemble, MAP and BP thresholds are associated with a rate  $R$  code ensemble that also share some structural properties (e.g. LDPC code ensemble specified by a degree distribution for variable and check nodes). For the given code ensemble, MAP threshold is the fundamental limit that one can hope to achieve with this ensemble. However in practice, MAP threshold might not be achievable and hence one settles for BP threshold that corresponds to the limit achievable via BP decoding. While finding the Shannon and BP thresholds are possible, finding the MAP threshold, in general, is known to be computationally prohibitive [1]–[3]. While spatial coupling strategies provides a way to approach this fundamental limit via BP decoding [4]–[10], this approach is computationally cumbersome. Apart from theoretical interests, therefore the problem of estimating the MAP threshold is very important.

Méasson et al. [2], [11] have proposed an analytical method to estimate the MAP threshold of LDPC and parallel

turbo codes over any binary memoryless symmetric (BMS) channel. In this method, the MAP threshold is obtained by applying the *Maxwell construction* to the EBP-GEXIT chart of the given code ensemble (details can be found in [1, Sec. 3.20], [3]). While finding this EBP-GEXIT chart is possible for the BEC, obtaining it for general BMS channels becomes computationally prohibitive for numerically involved codes such as generalized LDPC (GLDPC), doubly generalized LDPC (DGLDPC), and serially-concatenated turbo-codes (SC-TC). One can also estimate the MAP threshold of the given uncoupled code by finding the BP threshold of its spatially-coupled version of large enough length (this phenomenon is termed as *threshold saturation*). However this threshold saturation is guaranteed only when the length of the code tends to infinity and for finite length case, one needs to validate the estimated MAP threshold with respect to the MAP threshold estimated analytically. It is thus desirable to provide a computationally tractable analytical method for estimating the MAP threshold.

In this work, we provide a method for obtaining an approximate EBP-GEXIT chart of the given code ensemble, which is then used to estimate the MAP threshold via Maxwell construction. In our conference papers [12] and [13], we have proposed a method to find an approximate EBP-GEXIT chart for LDPC/GLDPC/DGLDPC codes and SC-TC respectively over binary-input AWGN (BAWGN). In this paper, we extend this method for non-binary complex-input AWGN channel, which in turn allows us to incorporate the system when codewords are modulated by any arbitrary modulation scheme. The main contributions of our work are summarized below.

- We first consider the system when codewords are mapped according the Gray mapping. In this case, we consider the equivalent bit-interleaved coded-modulation (BICM) channel and provide a method to find an approximate EBP-GEXIT chart (see Section III, [12], [13]).
- We then consider the system when codewords are mapped according to an arbitrary mapping. In this case, we first derive an expression for the GEXIT function (by extending the results of [2], [14]) and then provide a method for its tractable estimation (see Section IV, Theorems 1 and 2).
- The key idea of our method consists of making use of

the consistent Gaussian assumption for all the densities involved in computation of the GEXIT function. This enables us to compute the EBP-GEXIT chart banking upon the EXIT charts of the constituent codes, which are much easier to find and are typically known.

- Finally, we provide a detailed complexity analysis comparing the computation cost of finding the EBP-GEXIT chart via its direct computation versus our simplified method (see Section V, Propositions 1 and 2).
- The numerical results consists of MAP threshold estimates for a variety of LDPC, GLDPC, DGLDPC, and SC-TC ensembles. As an illustration of validity of our method, we also verify our estimated MAP thresholds of SC-TC ensembles via spatial coupling.

## II. SYSTEM MODEL AND PRELIMINARIES

### A. System model

LDPC( $\lambda, \rho$ ) denotes LDPC code ensemble, where  $\lambda(x) = \sum_i \lambda_i x^{i-1}$  and  $\rho(x) = \sum_j \rho_j x^{j-1}$  denote the edge perspective degree distributions for variable nodes (VNs) and check nodes (CNs) respectively [1]. Let  $\Lambda(x)$  and  $P(x)$  be the corresponding node perspective degree distribution pairs for VNs and CNs respectively. While for LDPC codes, every CN operation correspond to a single parity check code and every VN operation corresponds to a repetition code, for GLDPC codes some of the CN operations correspond to an arbitrary linear code and for DGLDPC codes both VN and CN operations correspond to a general linear code [15]. We assume that all VNs are unpunctured and have degrees strictly greater than one. For SC-TC, we denote the outer and inner convolutional codes by  $\mathcal{O}$  and  $\mathcal{J}$  respectively and the corresponding ensemble by  $\mathcal{S}(\mathcal{O}, \mathcal{J})$ .

We consider the digital communication system illustrated in Fig. 1. The binary channel code used at the transmitter is either an LDPC code or SC-TC. Message bit sequence  $\mathbf{b}$  is encoded to get a codeword sequence  $\mathbf{c} = [c_1 c_2 \dots c_n]$  of length  $n$ . The encoded bits are then interleaved to get an interleaved sequence of codebits  $\mathbf{c}' = [c'_1 c'_2 \dots c'_n]$ . For a  $2^m$ -ary modulation scheme, coded bit sequence  $\mathbf{c}'$  is first divided into  $N = n/m$  vectors each of length  $m$  and denoted by  $\mathbf{c}' = [\mathbf{c}'(1) \mathbf{c}'(2) \dots \mathbf{c}'(N)]$ , where  $\mathbf{c}'(t) = [c'_{(t-1)m+1} c'_{(t-1)m+2} \dots c'_{tm}]$  for  $t = 1, 2, \dots, N$ . Let us denote the entries in  $\mathbf{c}'(t)$  as  $\mathbf{c}'(t) = [c'_{t,1} c'_{t,2} \dots c'_{t,m}]$ . Modulated symbols are denoted by  $\mathbf{x} = [x_1 x_2 \dots x_N]$ , where each  $x_t$  is a complex modulated symbol corresponding to  $\mathbf{c}'(t)$ . Let  $\mathbb{X} = \{\xi_1, \xi_2, \dots, \xi_{|\mathbb{X}|}\}$  denotes the set of complex constellation symbols. The constellation of modulated symbols can be labeled according to any arbitrary mapping rule.

The noise is introduced by non-binary complex-input AWGN channel with variance  $\sigma^2$ . The noise affected version  $y_t$  of the  $t$ -th transmitted symbol  $x_t$  is given by  $y_t = x_t + n_t$ , where each noise sample  $n_t$  is chosen independently and identically distributed (i.i.d.) according to the complex normal distribution  $\mathcal{CN}(0, \sigma^2)$ , for  $t = 1, 2, \dots, N$ . In this work, it is convenient to parameterize the channel using its entropy, denoted by  $h = H(X)$ , ( $h \in [0, |\mathbb{X}|]$ ) [16].

The family of AWGN channels parameterized by  $h$  is denoted by  $\{\text{AWGN}(h)\}_h$  and as in [1], [2], we assume that  $\{\text{AWGN}(h)\}_h$  is ordered by physical degradation and it is smooth with respect to  $h$ . At the receiver, detector computes the sequence  $\mathbf{L}'$  of log-likelihood ratios (LLR) of the interleaved bit sequence  $\mathbf{c}'$  and  $i$ -th entry in  $\mathbf{L}'$  is given by  $L'_i := \log \frac{\mathbb{P}[c'_i=0|y]}{\mathbb{P}[c'_i=1|y]}$ , for  $i = 1, 2, \dots, n$ . The deinterleaved LLR sequence  $\mathbf{L}$  is then given to the channel decoder to get decoded message bits  $\hat{\mathbf{b}}$ . Note that in practice, iterative schemes are considered within the channel decoder (in the case of LDPC or SC-TC) or between the detector and the decoder (in the case of BICM).

For BMS channels, the input alphabet set is given by  $\mathbb{X} = \{+1, -1\}$  and in this case, the distribution of  $\mathbf{L}$  under the condition  $X = +1$  is referred to as  $L$ -density, denoted by  $c_{BMS(h)}$  [2, Sec. II]. For the BAWGN channel, the  $L$ -density is given by  $c_{BAWGN(h)} = \mathcal{N}(2/\sigma^2, 4/\sigma^2)$  [1, Ex. 4.21] and its entropy  $H(c_{BAWGN(h)})$  is given by [2, Sec. II],

$$\begin{aligned} H(c_{BAWGN(h)}) &= \int_{-\infty}^{\infty} \frac{\exp\left[-\frac{(l-(2/\sigma^2))^2}{8/\sigma^2}\right]}{\sqrt{2\pi(4/\sigma^2)}} \log_2(1 + e^{-l}) dl \\ &=: 1 - J(2/\sigma), \end{aligned} \quad (1)$$

where the definition of function  $J(\cdot)$  is inspired from [17]. Channel with non-binary inputs is known to be asymmetric and  $L$ -density cannot be defined in this case [18] and entropy of such channels is computed numerically ([14, Sec.III-A]).

### B. EBP-GEXIT charts of LDPC codes over BAWGN [2]

We first recall density evolution (DE) equations for the BP decoding of LDPC codes. The DE equations for LDPC( $\lambda, \rho$ ) code ensemble are given by [1, Thm. 4.97, Sec. 4.5.2]

$$a^{BP,l} = c_{BAWGN(h)} \star \lambda(\rho(a^{BP,l-1})), \quad (2)$$

where  $a^{BP,l}$  is the density of a randomly chosen VN or CN message in the  $l$ -th iteration of BP decoding,  $\lambda(a) = \sum_i a^{\star(i-1)}$ , and  $\rho(a) = \sum_i a^{\circledast(i-1)}$ . The operators  $\star$  and  $\circledast$  denote the convolutions over  $\mathbb{R}$  and the group  $\mathbb{F}_2 \times [0, +\infty]$  respectively [1, Sec. 4.1.4]. The operations  $a^{\star(i-1)}$  and  $a^{\circledast(i-1)}$  denote the respective convolutions of density  $a$  with itself  $(i-1)$  times.

For defining the EBP-GEXIT chart, we need to consider a *complete fixed-point (FP) family* [2, Sec. VII-A]. The family of densities  $\{a_x\}_x$  and  $\{c_x\}_x$  parameterized by  $x \in [0, 1]$  is called a complete FP family if (i)  $c_x \in \{\text{BAWGN}(h)\}_h$  for some  $h \in [0, 1]$ , (ii) for any  $x \in [0, 1]$ ,  $a_x = c_x \star \lambda(\rho(a_x))$  ( $\{a_x, c_x\}$  is a FP density pair), (iii)  $H(a_x) = x$ , and (iv)  $\{a_x\}_x$  and  $\{c_x\}_x$  are smooth with respect to  $x$ . The EBP-GEXIT function  $g^{EBP}(x)$  for LDPC( $\lambda, \rho$ ) is defined as

$$g^{EBP}(x) := \int_{-\infty}^{\infty} \Lambda(\rho(a_x))(z) l^{c_x}(z) dz, \quad (3)$$

where  $l^{c_x}(z)$  is called the GEXIT kernel [1, Ch.4]. For the BAWGN channel with  $L$ -density  $c_{BAWGN(h)} =$

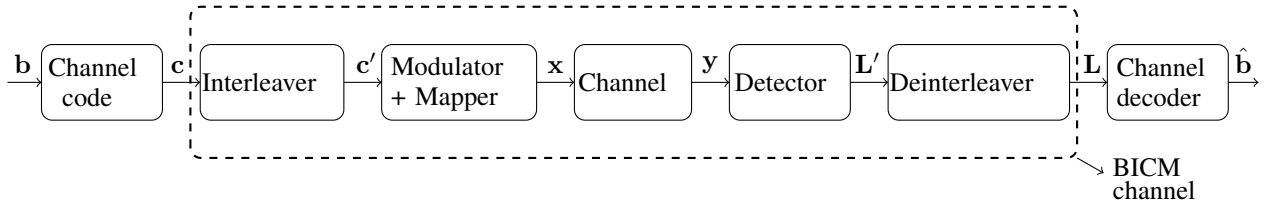


Fig. 1: Block diagram of a digital communication system considered in this paper.

$\mathcal{N}(2/\sigma^2, 2/\sigma^2)$ , an expression for  $l^{c_{BAWGN}(h)}(z)$  is given by [2, Example 7]

$$l^{c_{BAWGN}(h)}(z) = \left( \int_{-\infty}^{\infty} \frac{e^{-\frac{(w-(2/\sigma^2))^2}{8/\sigma^2}}}{1+e^{w+z}} dw \right) / \left( \int_{-\infty}^{\infty} \frac{e^{-\frac{(w-(2/\sigma^2))^2}{8/\sigma^2}}}{1+e^w} dw \right). \quad (4)$$

The EBP-GEXIT chart is the curve obtained by plotting  $g^{EBP}(x)$  versus  $c_x \forall x \in [0, 1]$ .

### III. EBP-GEXIT CHART OVER THE AWGN CHANNEL WITH GRAY MAPPING

In this section, we consider the situation when modulated symbols are mapped according to the Gray mapping and study the situation of any arbitrary mapping in the next section.

#### A. Equivalent bit-channels for Gray mapping

In the presence of an interleaver between the channel coded bits and the modulator, in Fig. 1 one can consider an equivalent channel, termed as the *BICM channel*, formed by the interleaver, modulator, AWGN channel, detector, and deinterleaver [16]. For obtaining the EBP-GEXIT chart, we parameterize this BICM channel by its entropy  $h$ , denoted as  $BICM(h)$ . An ideal interleaver implies that the set of random variables corresponding to  $\{L_1, L_2, \dots, L_n\}$  are independent and hence this BICM channel can be equivalently seen as a set of  $n$  parallel independent BMS [19]. While for some modulation schemes (such as BPSK) the exact distribution of each  $L_i$  is known, finding this distribution for an arbitrary modulation scheme may become difficult. Hence in the literature good approximations for its distribution are suggested [20]–[23]. Typically for the Gray mapping, the density  $c_{BICM(h)}$  of a randomly chosen  $L_i$  can be well approximated by a mixture of consistent Gaussian densities. For an integer  $M$  suppose  $c_{BICM(h)}$  is given by

$$c_{BICM(h)} = \sum_{j=1}^M d_j \mathcal{N}(l_j, 2l_j), \quad (5)$$

where  $l_j$  is the mean of the  $j$ -th constituent density and each  $d_j \in [0, 1]$  such that  $d_1 + \dots + d_M = 1$ . This implies that  $H(c_{BICM(h)}) = \sum_{j=1}^M d_j [1 - J(\sqrt{2l_j})]$ . While for BPSK we have  $M = 1, d_1 = 1$  and  $l_1 = 2/\sigma^2$ , for other modulation schemes we use the approximations suggested in [23].

#### B. EBP-GEXIT chart for GLDPC/DGLDPC codes over the BICM channel

We first extend the EBP-GEXIT chart proposed for LDPC codes over BAWGN channel to GLDPC and DGLDPC over BICM channel. Let  $f_C(\cdot)$  and  $f_V(\cdot)$  be the density transfer functions corresponding to CN and VN processing respectively. Then similar to Eq. (2), the DE equation is given by  $a^{BP,l} = c_{BICM(h)} \star f_V(f_C(a^{BP,l-1}))$ . Note that for an irregular LDPC code,  $f_C(\cdot) = \rho(\cdot)$  and  $f_V = \lambda(\cdot)$  [1, Thm. 4.97] and for GLDPC and DGLDPC codes,  $f_C(\cdot)$  and  $f_V(\cdot)$  need to be obtained numerically [24], [25]. To find a FP density pair corresponding to the given BICM channel with the  $L$ -density  $c_{BICM(h)}$ , we need to find all possible densities  $a$  that satisfy

$$a = c_{BICM(h)} \star f_V(f_C(a)). \quad (6)$$

For the given fixed-density pair  $\{a, c_{BICM(h)}\}$ , the EBP-GEXIT function is given by

$$g^{EBP}(h) := \int_{-\infty}^{\infty} \Lambda(f_C(a))(z) l^{c_{BICM(h)}}(z) dz, \quad (7)$$

where  $l^{BICM(h)}(z)$  is the GEXIT kernel for  $BICM(h)$ . From Eq. (5) we have  $l^{c_{BICM(h)}}(z) = \sum_{j=1}^M a_j l^{c_{BAWGN}(h_j)}(z)$ , where  $h_j = 1 - J(\sqrt{2l_j})$  and  $l^{c_{BAWGN}(h_j)}(z)$  is defined in Eq. (4).

For tractable computation of the EBP-GEXIT chart, we next find Eq. (6) and Eq. (7) efficiently.

##### 1) Numerical computation of FP density in Eq. (6):

We assume that the density  $a$  in Eq. (6) is consistent normal, i.e.,  $a = \mathcal{N}(m_a, 2m_a)$  for some real number  $m_a$ . This consistent Gaussian assumption proposed by Chung et al. [26] is also used for classical EXIT charts analysis [17]. Using the consistent Gaussian assumption for  $a$  is the key idea that simplifies the operations required towards finding the EBP-GEXIT curve. Similar to the EXIT-chart analysis, we consider the mutual information (MI)  $I_{E_v}$  between the LLRs and their corresponding VNs bits. It is given by  $I_{E_v} = J(\sqrt{2m_a})$  where  $2m_a$  is the variance of the density  $a$  and  $J(\cdot)$  is defined in Eq. (1). Since  $J(\cdot)$  is a one-to-one function, the density  $a$  can be uniquely determined from it. Similarly, let  $I_{E_c}$  be the MI corresponding to the density  $f_C(a)$  and suppose  $I_{E_c} = \Gamma^C(I_{E_v})$ , where  $\Gamma^C(\cdot)$  is the MI transfer function corresponding to CN processing. Note that in notation  $\Gamma^C(\cdot)$ , we have used the alphabet  $\Gamma$  to indicate the MI transfer function and the superscript  $C$  for the CN processing. The MI corresponding to the VN to CN message is a function of  $h$  and  $I_{E_c}$ , denoted by  $\Gamma^V(I_{E_c}, h)$ .

Using this the FP density equations Eq. (6) can be efficiently approximated using a classical EXIT-like mono-dimensional FP equation as

$$I_{E_v} = \Gamma^V \left( \Gamma^C(I_{E_v}), h \right). \quad (8)$$

The FP density pairs now consists of all those consistent normal densities  $a$  such that the corresponding  $I_{E_v} = J(\sqrt{2m_a})$  satisfy Eq. (8). Observe that the FP density in Eq. (6) is now represented by a FP equation Eq. (8) since both  $I_{E_v}$  and  $h$  are scalars. All possible pairs  $\{a, c_{BICM(h)}\}$  that satisfy Eq. (6) can be found efficiently via a grid search by varying  $I_{E_v}$  and  $h$  in the range  $[0, 1]$ . For LDPC codes,  $\Gamma^C(\cdot)$  and  $\Gamma^V(\cdot, \cdot)$  can be simplified as

$$\begin{aligned} \Gamma^C(I_{E_v}) &= \sum_j \rho_j \left( 1 - J \left[ \sqrt{(j-1)[J^{-1}(1-I_{E_v})]^2} \right] \right) \\ \Gamma^V(I_{E_c}, h) &= \sum_i \lambda_i \sum_{j=1}^M d_j J \left[ \sqrt{(i-1)[J^{-1}(I_{E_c})]^2 + 2l_j} \right], \end{aligned} \quad (9)$$

where  $I_{E_c} = \Gamma^C(I_{E_v})$  and  $2l_j$  is the variance of the  $j$ -th constituent density in the mixture  $c_{BICM(h)}$ . For GLDPC and DGLDPC codes,  $\Gamma^C(\cdot)$  and  $\Gamma^V(\cdot, \cdot)$  are evaluated point-wise by means of Monte Carlo simulations and stored before computation of Eq. (8) [24], [25].

2) *Numerical computation of the EBP-GEXIT function provided in Eq. (7)* : For the given  $BICM(h)$ , let  $\mathcal{S}_h$  be the set of all possible  $I_{E_v} \in [0, 1]$  that satisfy Eq. (8). Recall that corresponding to each  $I_{E_v}$  there is a density  $a = \mathcal{N}(m_a, 2m_a)$  with  $I_{E_v} = J(\sqrt{2m_a})$ . Each  $a$  corresponding to  $I_{E_v} \in \mathcal{S}_h$  provides a point on the EBP-GEXIT curve that is computed using Eq. (7). We now provide tractable computation of these equations. We first explain calculations towards  $\Lambda(f_C(a))$  under our Gaussian assumption. For any  $I_{E_v} \in \mathcal{S}_h$ , suppose  $I_{E_c} = \Gamma^C(I_{E_v})$  and  $m_b = [J^{-1}(I_{E_c})]^2/2$ . This implies that the density  $f_C(a)$  is consistent Gaussian with mean  $m_b$ , i.e.,  $f_C(a) = \mathcal{N}(m_b, 2m_b)$ . For a VN of degree  $j$ , the density obtained by taking the convolution of the input density  $j$  times is also a consistent Gaussian density of mean  $jm_b$ . Let us denote this density by  $b_j = \mathcal{N}(jm_b, 2jm_b)$ . The density  $\Lambda(f_C(a))$  is thus the mixture of densities  $b_j$  given by  $\Lambda(b)(f_C(a)) = \sum_j \Lambda_j b_j(z)$ . Substituting this in Eq. (7) we get,

$$\begin{aligned} g^{EBP}(h) &= \int_{-\infty}^{\infty} \left[ \sum_j \Lambda_j b_j(z) \right] l^{c_{BICM(h)}}(z) dz \\ &= \sum_j \Lambda_j \mathbb{E}_{b_j} \left[ l^{c_{BICM(h)}}(z) \right], \end{aligned} \quad (10)$$

where  $\mathbb{E}_{b_j}[\cdot]$  is now expectation over the Gaussian density  $b_j$ . The expectation  $\mathbb{E}_{b_j}[l^{c_{BICM(h)}}(z)]$  can be computed efficiently using the Gauss-Hermite quadrature weights as follows [27]:

- Let  $H_d$  be the Hermite polynomial of degree  $d$  with roots  $k_1, k_2, \dots, k_d$ , for some  $d \in \mathbb{Z}$ .
- Let  $z_i = \sqrt{4jm_b}k_i + jm_b$ . Then an approximate value

of  $\mathbb{E}_{b_j}[l^{c_{BICM(h)}}(z)]$  is given by

$$\begin{aligned} &\mathbb{E}_{b_j} \left[ l^{c_{BICM(h)}}(z) \right] \\ &\approx \frac{1}{\sqrt{\pi}} \sum_{i=1}^d \frac{2^{d-1} d! \sqrt{\pi}}{d^2 [H_{d-1}(k_i)]^2} l^{c_{BICM(h)}}(z_i), \end{aligned} \quad (11)$$

where  $l^{c_{BICM(h)}}(z_i)$  is defined in Eq. (7) and can either be computed using numerical integration or using our approximations provided in Appendix C.

To summarize, the consistent Gaussian assumption enables the computation of the complete FP family (via grid search) and the evaluation of the EBP-GEXIT function (via Gauss-Hermite quadrature weights) computationally feasible. Detailed steps are provided in Algorithm 1.

---

#### Algorithm 1 Numerical computation of EBP-GEXIT chart

---

- 1) **Choose**  $h \in [0, 1]$  and let  $c_{BICM(h)}$  be the  $L$ -density corresponding to  $BICM(h)$ .
  - 2) **Find**  $\mathcal{S}_h := \{I_{E_v} : \text{s.t. } I_{E_v} \text{ satisfies Eq. (8)}\}$ , via grid search of  $I_{E_v}$  in the range  $[0, 1]$ .
  - 3) **Compute**  $g^{EBP}(h)$  using Eq. (10) for the set of densities  $a$  corresponding to each  $I_{E_v} \in \mathcal{S}_h$ .
  - 4) **Plot** all possible values  $g^{EBP}(h)$  obtained in step (3) versus the chosen  $h$ .
  - 5) **Repeat** the process for various values of  $h \in [0, 1]$ .
- 

**Remark 1.** In Algorithm 1 instead of using a grid search, one can approximate the function  $\Gamma^V(\Gamma^C(I_{E_v}), h)$  and use zero-crossing algorithms to find the complete fixed-point family. Further, instead of following the procedure given in Algorithm 1, one can also use the procedure provided in [2, Sec. VIII] along with our proposed simplifications to obtain the EBP-GEXIT chart.  $\square$

**Remark 2.** On contrary to the definition of complete FP family (see Section II-B),  $a$  and  $c_{BICM(h)}$  pairs obtained using Algorithm 1 are not parameterized by some  $x \in [0, 1]$ , since we find these pairs exhaustively. However it can be easily verified that  $H(a) = x$  for some  $x \in [0, 1]$  and the set of  $a$  and  $c_{BICM(h)}$  obtained do form a complete FP family.  $\square$

**Remark 3.** The EBP-GEXIT chart for SC-TC can be obtained in a similar way as that of Section III-B and we skip the details (details can be found in [13]).  $\square$

#### IV. EBP-GEXIT CHART OVER THE AWGN CHANNEL WITH NON-GRAY MAPPING

We now consider the case when modulated symbols are mapped according to any non-Gray mapping. Note that for any non-Gray mapping, the EXIT chart of the detector is not flat and hence decoding of the system illustrated in Fig. 1 becomes doubly iterative [28]. Thus for LDPC codes one needs to iterate between VNs and CNs but also between detector and decoder (similarly for SC-TC). Hence for computing the EBP-GEXIT chart we need to consider complex-input AWGN channel. We first extend the existing results to obtain an expression for the GEXIT function for

non-binary AWGN channel and then provide its tractable computation method.

### A. GEXIT function for non-binary complex-input AWGN channel

We use of the definition of the GEXIT function [2] and extend the approach of [14] to derive an expression for the GEXIT function for non-binary complex-input AWGN channel. We first introduce some notation. Corresponding to the  $t$ -th transmitted symbol  $x_t \in \mathbb{X}$ ,  $\phi_t$  is defined as

$$\phi_t := \left[ \mathbb{P}(X_t = \xi_1 | \mathbf{y}_{\sim t}) \quad \dots \quad \mathbb{P}(X_t = \xi_{|\mathbb{X}|} | \mathbf{y}_{\sim t}) \right] \quad (12)$$

where  $\mathbf{y}_{\sim t} = [y_1 \dots y_{t-1} y_{t+1} \dots y_N]$ . Let  $\Phi_t$  be the random vector corresponding to  $\phi_t$ . Let  $f_{t,\xi}$  be the distribution of  $\Phi_t$  under the condition  $X_t = \xi$ , i.e.,  $f_{t,\xi}(\phi_t) := \mathbb{P}[\Phi_t = \phi_t | X_t = \xi]$ , where  $\xi \in \mathbb{X}$ . The entry in  $\phi_t$  corresponding to  $\xi$  is denoted by  $\phi_{t,[\xi]}$ , i.e.,  $\phi_{t,[\xi]} := \mathbb{P}(X_t = \xi | \mathbf{y}_{\sim t})$ .

Observe that  $\phi_t$  corresponds to the likelihood of  $X_t$  given all received symbols except the  $t$ -th symbol. In the presence of an ideal interleaver between channel code and modulator (see Fig. 1), interleaved codebits can be assumed to be independent and as a consequence,  $X_1, X_2, \dots, X_N$  can be assumed to be independent. Since modulated symbols are passed through memoryless AWGN channel,  $\mathbb{P}(X_t = \xi | \mathbf{Y}_{\sim t}) = \mathbb{P}(X_t = \xi)$  and hence the likelihood of  $X_t$  will depend on the *a priori* knowledge available about it<sup>1</sup>. We next obtain a general expression for the GEXIT function and later make use of this independent assumption for its numerical computation.

**Theorem 1.** Consider  $\phi_t, f_{t,\xi}(\phi)$ , and  $\phi_{t,[\xi]}$  as defined above (see Eq. (12)). Then the GEXIT function  $g(h)$  for  $|\mathbb{X}|$ -ary complex-input memoryless AWGN channel with entropy  $h$  is given by  $g(h) = \frac{1}{N} \sum_{t=1}^N \frac{A_t(h)}{B_t(h)}$ , where  $A_t(h)$  and  $B_t(h)$  are given by

$$A_t(h) = \sum_{\xi \in \mathbb{X}} \int_{\phi_t} f_{t,\xi}(\phi_t) \int_{y_t} \frac{e^{-\frac{|y_t - \xi|^2}{2\sigma^2}}}{2\pi\sigma^2} [|y_t - \xi|^2 - 2\sigma^2]$$

$$\log_2 \left\{ \sum_{\xi' \in \mathbb{X}} \frac{\phi_{t,[\xi']}}{\phi_{t,[\xi]}} \exp \left[ \frac{|y_t - \xi|^2 - |y_t - \xi'|^2}{2\sigma^2} \right] \right\} dy_t d\phi$$

$$B_t(h) = \sum_{\xi \in \mathbb{X}} \int_{y_t} \frac{e^{-\frac{|y_t - \xi|^2}{2\sigma^2}}}{2\pi\sigma^2} [|y_t - \xi|^2 - 2\sigma^2]$$

$$\log_2 \left\{ \sum_{\xi' \in \mathbb{X}} \exp \left[ \frac{|y_t - \xi|^2 - |y_t - \xi'|^2}{2\sigma^2} \right] \right\} dy_t.$$

The proof is given in Appendix A. The fraction  $g_t(h) := A_t(h)/B_t(h)$  in Theorem 1 is termed as the  $t$ -th GEXIT function [14]. We next find the EBP-GEXIT function. Similar to Eq. (12), consider  $\Phi_t^{BP,l}$  corresponding to the likelihood of  $X_t$  given  $\mathbf{y}_{\sim t}$  in the  $l$ -th round of BP decoding and let  $f_{t,\xi}^{BP,l}$  be the density of  $\Phi_t^{BP,l}$  under the condition  $X_t = \xi$ . The BP-GEXIT function  $g^{BP,l}(h)$  in the  $l$ -th round

<sup>1</sup>For an iterative system, the distribution of  $X_t$  will depend on the output from the channel decoder in the previous iteration.

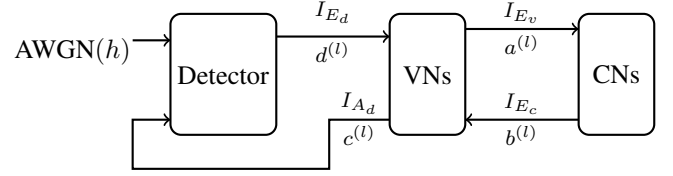


Fig. 2: Considered decoding scheduling for the LDPC-coded serially concatenated scheme

of BP-decoding is obtained by substituting  $f_{t,\xi} = f_{t,\xi}^{BP,l}$  in Theorem 1 and the BP-GEXIT function is defined as  $g^{BP}(h) := \lim_{l \rightarrow \infty} g^{BP,l}(h)$  [2]. The EBP-GEXIT function is obtained by computing  $g^{BP}(h)$  for each FP density pair. To apply Maxwell construction, we next provide the area theorem for  $|\mathbb{X}|$ -ary complex-input AWGN channel.

**Theorem 2.** Consider a family of channel codes of rate  $k/n$  and transmission using the digital communication system of Fig. 1 over  $\{AWGN(h)\}_h$  using  $2^m$ -ary modulation scheme. Then

$$\frac{1}{m} \int_0^m g(h) dh = \frac{k}{n}.$$

The proof is given in Appendix B.

### B. Numerical computation of the complete FP family

To find complete FP family for LDPC codes, we need to consider the DE equations of the system illustrated in Fig. 2. In one iteration of decoding, first a message is passed from the detector to VNs. VNs then pass messages to CNs, which are then passed back to VNs after CN processing. Finally, an average message from VNs is sent back to the detector. This scheduling is in spirit equivalent to the combined VN and detector approach of [29, Fig. 5]). Let  $a^{(l)}, b^{(l)}, c^{(l)}$ , and  $d^{(l)}$  be the respective densities of these messages and using this DE equations will be

$$a^{(l)} = d^{(l-1)} \star f_V(b^{(l-1)}), \quad b^{(l)} = f_C(a^{(l)})$$

$$c^{(l)} = f_V'(b^{(l)}), \quad d^{(l)} = f_D(c^{(l)}, h), \quad (13)$$

where the function  $f_D(\cdot, \cdot)$  depends on the underlying detector and channel parameter  $h$ ,  $f_V'(\cdot)$  correspond to the VN-to-detector processing and recall that  $f_V(\cdot)$  and  $f_C(\cdot)$  correspond to VN and CN processing respectively. In (13) when  $a^{(l)} = a^{(l-1)}$  then such a density will be a FP density, i.e., for the given  $h$  the density  $a$  is called as FP density if it satisfies

$$a = f_D\left(f_V'(f_C(a)), h\right) \star f_V\left(f_C(a)\right). \quad (14)$$

Similar to Section III-B1, we project the densities in (13) on their respective MIs ( $I_{E_v}, I_{E_c}, I_{A_d}$ , and  $I_{E_d}$ ) and use MI transfer functions ( $\Gamma^V(\cdot), \Gamma^C(\cdot), \Gamma^{V'}(\cdot)$ , and  $\Gamma^D(\cdot)$ ) to find the FP equation corresponding to Eq. (14) as follows

$$I_{E_v} = \Gamma^V\left(\Gamma^C(I_{E_v}), \Gamma^D\left(\Gamma^{V'}(\Gamma^C(I_{E_v})), h\right)\right). \quad (15)$$

Similar to Section III-B1, all possible pairs  $a$  and  $h$  that satisfy FP density in Eq. (14) can be found efficiently from

Eq. (15) via grid search by varying  $I_{E_v}$  and  $h$  in the ranges  $[0, 1]$  and  $[0, H(X)]$  respectively (recall that  $H(X)$  is the entropy of non-binary AWGN channel).

### C. Numerical computation of the EBP-GEXIT function

We now provide a method for numerical computation of the GEXIT function derived in Theorem 1. In this theorem, as the expression for  $A_t(h)$  and  $B_t(h)$  is the same for  $t = 1, 2, \dots, N$ , we get  $A_1(h) = \dots = A_N(h) = A(h)$  and  $B_1(h) = \dots = B_N(h) = B(h)$  and hence  $g(h) = \frac{1}{N} \sum_{t=1}^N \frac{A_t(h)}{B_t(h)} = \frac{A(h)}{B(h)}$ . For the sake of convenience, we drop the suffix  $t$  from the expression of  $A_t(h)$  and  $B_t(h)$ . We remove the suffix  $t$  from the terms  $f_{t,\xi}(\phi_t)$ ,  $\Phi_t$ , and  $Y_t$  as well. Let us denote the term inside the integration with respect to  $y$  in the expression of  $A(h)$  by  $R_1(y, \phi, \xi, \sigma)$ , i.e.,

$$R_1(y, \phi, \xi, \sigma) := [|y - \xi|^2 - 2\sigma^2] \log_2 \left\{ \sum_{\xi' \in \mathbb{X}} \frac{\phi[\xi']}{\phi[\xi]} \exp \left[ \frac{|y - \xi|^2 - |y - \xi'|^2}{2\sigma^2} \right] \right\}. \quad (16)$$

Using this  $A(h)$  can be written as

$$\begin{aligned} A(h) &= \sum_{\xi \in \mathbb{X}} \int_{\phi} f_{\xi}(\phi) \int_y \frac{e^{-\frac{|y-\xi|^2}{2\sigma^2}}}{2\pi\sigma^2} R_1(y, \phi, \xi, \sigma) dy d\phi, \\ &\stackrel{(a)}{=} \sum_{\xi \in \mathbb{X}} \int_{\phi} f_{\xi}(\phi) \left( \mathbb{E}_{Y|X=\xi} [R_1(Y, \phi, \xi, \sigma)] \right) d\phi \\ &\stackrel{(b)}{=} \sum_{\xi \in \mathbb{X}} \mathbb{E}_{\Phi|X=\xi} [R_2(\Phi, \xi, \sigma)], \end{aligned} \quad (17)$$

where  $R_2(\Phi, \xi, \sigma) := \mathbb{E}_{Y|X=\xi} [R_1(Y, \phi, \xi, \sigma)]$ . The equality in (a) is obtained since the integration with respect to  $y$  is equal to the expectation of  $R_1(y, \phi, \xi, \sigma)$  with respect to random variable  $Y|X = \xi$ . The equality in (b) is obtained since the integration with respect to  $\phi$  is equal to the expectation of  $R_2(\phi, \xi, \sigma)$  with respect to the random vector  $\Phi$  under the condition  $X = \xi$ . For computing  $A(h)$ , the key step now is to compute  $R_2(\phi, \xi, \sigma)$  and its expectation with respect to random variable  $\Phi|X = \xi$ . These computations are described next.

- Computing  $R_2(\phi, \xi, \sigma)$  defined in Eq. (17): The function  $R_2(\phi, \xi, \sigma)$  is given by

$$R_2(\phi, \xi, \sigma) = \int_y \frac{e^{-\frac{|y-\xi|^2}{2\sigma^2}}}{2\pi\sigma^2} R_1(y, \phi, \xi, \sigma) dy \quad (18)$$

Observe that the distribution of complex random variable  $Y$  under the condition  $X = \xi$  is bivariate Gaussian with mean  $\xi$  and variance  $\sigma^2$ . This expectation can be computed efficiently via two-dimensional Gauss-Hermite quadrature weights as follows [30]:

- Suppose  $\xi = \xi^r + i\xi^i$  where  $\xi^r$  and  $\xi^i$  are the real and imaginary parts of  $\xi$ .
- Let  $H_d$  be the Hermite polynomial of degree  $d$  with roots  $k_1, k_2, \dots, k_d$ .
- Let  $z(j_1, j_2) = [\sqrt{2\sigma}k_{j_1} + \xi^r] + i[\sqrt{2\sigma}k_{j_2} + \xi^i]$ ,  $w_{j_1} = 2^{d-1}d!\sqrt{\pi}/d^2[H_{d-1}(k_{j_1})]^2$ , and

$w_{j_2} = 2^{d-1}d!\sqrt{\pi}/d^2[H_{d-1}(k_{j_2})]^2$  for  $j_1, j_2 = 1, 2, \dots, d$ . Then we have

$$R_2(\phi, \xi, \sigma) \approx \frac{1}{\pi} \sum_{j_1=1}^d \sum_{j_2=1}^d w_{j_1} w_{j_2} R_1[z(j_1, j_2), \phi, \xi, \sigma], \quad (19)$$

where  $R_1(z(j_1, j_2), \phi, \xi, \sigma)$  is defined in Eq. (16).

- Computing  $A(h)$ : Consider the vectors  $\Phi_1, \Phi_2, \dots, \Phi_N$  corresponding to  $X_1, X_2, \dots, X_N$  (see Eq. (12)). As explained in Section IV-A,  $\Phi_1, \Phi_2, \dots, \Phi_N$  can be assumed to be independent and without loss of generality we next provide computation steps for any  $i$ -th vector  $\Phi_i$ . Since  $\phi_i$  does not depend on  $\mathbf{y}_{\sim i}$ , Eq. (12) can be simplified to

$$\phi_i = \left[ \mathbb{P}(X_i = \xi_1) \quad \dots \quad \mathbb{P}(X_i = \xi_{|\mathbb{X}|}) \right]. \quad (20)$$

Recall that  $\mathcal{M}$  is the map corresponding to  $2^m$ -ary modulation scheme, i.e.,  $\mathcal{M} : \mathbf{c}'(i) \rightarrow x_i$ , where  $x_i \in \mathbb{X}$  and  $\mathbf{c}'(i) = [c'_{i,1} \ c'_{i,2} \ \dots \ c'_{i,m}]$  for  $i = 1, 2, \dots, N$  (see Section II). Let  $\mathbf{L}_a^{\mathcal{M}}(i) = [L_a^{\mathcal{M}}(i, 1) \ L_a^{\mathcal{M}}(i, 2) \ \dots \ L_a^{\mathcal{M}}(i, m)]$  be the *a priori* LLRs available at the input of the detector, which are obtained after deinterleaving VN-to-detector messages. Since  $\mathbf{c}(i) = [c_{i,1} \ c_{i,2} \ \dots \ c_{i,m}]$  denotes the deinterleaved codebit sequence, we have  $L_a^{\mathcal{M}}(i, j) = \log \frac{\mathbb{P}(C_{i,j}=0)}{\mathbb{P}(C_{i,j}=1)}$ , for  $j = 1, 2, \dots, m$ . For each  $\xi_l \in \mathbb{X} = \{\xi_1, \xi_2, \dots, \xi_{|\mathbb{X}|}\}$ , suppose  $\mathcal{M}^{-1}(\xi_l) = [b_{l,1} \ b_{l,2} \ \dots \ b_{l,m}]$  for  $l = 1, 2, \dots, |\mathbb{X}|$ . Then the  $l$ -th entry in  $\phi_i$  in Eq. (20) is computed as

$$\mathbb{P}(X_i = \xi_l) = \prod_{j=1}^m \mathbb{P}[C_{i,j} = b_{l,j}], \quad (21)$$

where  $\mathbb{P}[C_{i,j} = b_{l,j}]$  is obtained via  $L_a^{\mathcal{M}}(i, j)$ . To compute  $A(h) = \sum_{\xi \in \mathbb{X}} \mathbb{E}_{\Phi|X=\xi} [R_2(\Phi, \xi, \sigma)]$ , we need to find the distribution  $f_{\xi}(\phi)$  of  $\Phi|X = \xi$  (see Eq. (17)). However finding this multivariate distribution, in general, is not straightforward. Hence we choose to obtain this expectation numerically using  $\eta_m$  Monte Carlo points as follows:

- Let  $I_{A_d}$  be the MI available at the input of the detector (see Fig. 2). Project  $I_{A_d} \in [0, 1]$  on the consistent Gaussian density  $\mathcal{N}(m_d, 2m_d)$ , where  $m_d = J^{-1}(I_{A_d})^2/2$ .
- Generate a sequence of modulated symbols  $x_1, x_2, \dots, x_{\eta_m}$  according to uniform distribution for large enough  $\eta_m$ . (We choose  $\eta_m = 10000$  in our simulations.)
- Generate a sequence of *a priori* LLRs  $\mathbf{L}_a^{\mathcal{M}}(1), \mathbf{L}_a^{\mathcal{M}}(2), \dots, \mathbf{L}_a^{\mathcal{M}}(\eta_m)$  corresponding to  $x_1, x_2, \dots, x_{\eta_m}$ , where each entry in  $\mathbf{L}_a^{\mathcal{M}}(i) = [L_a^{\mathcal{M}}(i, 1) \ L_a^{\mathcal{M}}(i, 2) \ \dots \ L_a^{\mathcal{M}}(i, m)]$  is chosen i.i.d. according to  $\mathcal{N}(m_d, 2m_d)$  distribution.
- Compute the sequence of vectors  $\phi_1, \phi_2, \dots, \phi_{\eta_m}$ , where each entry in  $\phi_i$  is calculated from  $\mathbf{L}_a^{\mathcal{M}}(i)$  using Eq. (20) and Eq. (21), for  $i = 1, 2, \dots, \eta_m$ .

- Given a particular symbol  $\xi \in \mathbb{X}$ , let  $\mathcal{S}_\xi$  denotes the set of vectors  $\phi_i$  such that the corresponding generated  $x_i = \xi$  for  $i = 1, 2, \dots, \eta_m$ .
- From Eq. (17),  $A(h)$  is now approximated as  $A(h) \approx \sum_{\xi \in \mathbb{X}} \frac{1}{|\mathcal{S}_\xi|} \sum_{\phi_i \in \mathcal{S}_\xi} R_2(\phi_i, \xi, \sigma)$ , where  $R_2(\phi_i, \xi, \sigma)$  is computed using the steps discussed above.
- Computing  $B(h)$ : When  $\phi_{[\xi]} = \phi_{[\xi']}$  for any  $\xi, \xi' \in \mathbb{X}$ ,  $B(h)$  of Theorem 1 can be written in terms of  $R_2(\phi, \xi, \sigma)$  and computed as  $B(h) = \sum_{\xi \in \mathbb{X}} R_2\left(\phi = \left[\frac{1}{|\mathbb{X}|} \quad \frac{1}{|\mathbb{X}|} \quad \dots \quad \frac{1}{|\mathbb{X}|}\right], \xi, \sigma\right)$ .

## V. COMPLEXITY ANALYSIS

Recall that, obtaining the EBP-GEXIT chart consists of two main steps; finding the complete FP family and evaluating the GEXIT function. We now compare the complexity of performing these two steps using our proposed simplifications versus direct computations. Suppose we wish to find the FP family for LDPC codes, i.e., find all possible pairs of densities  $\{a, c_{BICM(h)}\}$  such that  $a = c_{BICM(h)} \star f_V(f_C(a))$ . With our simplifications, this problem gets reduced to finding all possible pairs of points  $\{I_{E_v}, h\}$  such that  $I_{E_v} = \Gamma^V(\Gamma^C(I_{E_v}), h)$  (see Section III-B1). While the solutions of  $I_{E_v} = \Gamma^V(\Gamma^C(I_{E_v}), h)$  can be obtained via grid-search (Remark 1), it is not possible to find the solutions of  $a = c_{BICM(h)} \star f_V(f_C(a))$  via such grid-search and one needs to follow the procedure of [2, Sec. VIII]. Since this procedure can also be applied to find the solutions of  $I_{E_v} = \Gamma^V(\Gamma^C(I_{E_v}), h)$ , for fair complexity comparison, we use it instead of grid-search. In this procedure, a real number  $x \in [0, 1]$  is chosen and the unique FP density pair  $\{a, c_{BICM(h)}\}$  parametrized by this  $x$  is obtained. For complexity comparison we focus on finding one FP density pair and evaluating the GEXIT function corresponding to it in Propositions 1 and 2.

**Proposition 1.** *Consider the system of LDPC/GDLPC/DGLDPC code with the Gray mapping. Suppose the FP density pair corresponding to the given  $x \in [0, 1]$  is obtained using the procedure given in [2, Sec. VIII]. Towards this, suppose we quantize and sample all densities into  $\eta_q$  points. Let  $\eta_m$  be the number of Monte Carlo points used to find the respective density transfer functions. Let  $\eta_v$  and  $\eta_c$  be the maximum number of states in the minimal canonical trellis of the constituent generalized VNs and CNs respectively. Then the complexity of finding the FP density pair with direct computation and with our simplifications is tabulated below:*

Code ensemble	Complexity with direct computation	Complexity with our simplifications
LDPC	$\mathcal{O}(\eta_q \log \eta_q)$	$\mathcal{O}(1)$
GLDPC	$\mathcal{O}(\eta_m 2^{\eta_c} + \eta_q \log \eta_q)$	$\mathcal{O}(1)$
DGLDPC	$\mathcal{O}(\eta_m (2^{\eta_c} + 2^{\eta_v}) + \eta_q \log \eta_q)$	$\mathcal{O}(1)$

*Proof:* The procedure of [2, Sec. VIII] for finding the FP density pair (corresponding to the given  $x$ ) primarily consists of performing the operation  $c_{BICM(h)} \star f_V(f_C(a))$

finite number of times. Thus the overall complexity of finding the FP density pair is equal to the complexity of the operation  $c_{BICM(h)} \star f_V(f_C(a))$  (which corresponds to performing  $\Gamma^V(\Gamma^C(I_{E_v}), h)$  in our simplified method). Thus for comparing the complexity of direct vs our simplified method, we need to compare the complexity of the operation  $c_{BAWGN(h)} \star f_V(f_C(a))$  versus  $\Gamma^V(\Gamma^C(I_{E_v}), h)$ .

For LDPC( $\lambda, \rho$ ) ensemble,  $c_{BICM(h)} \star f_V(f_C(a)) = c_{BICM(h)} \star \lambda(\rho(a))$  and computing this operation involves performing a set of convolutions over  $\mathbb{R}$  and  $\mathbb{F}_2 \times [0, +\infty]$  (see Eq. (2)). To compute these convolutions in practice, all the densities are sampled and quantized into  $\eta_q$  points and the convolutions are computed with the aid of  $\eta_q$ -point fast Fourier transforms (FFT) and inverse FFTs [15, Sec. 9.1]. Thus the complexity of operation  $c_{BICM(h)} \star \lambda(\rho(a))$  would be of the order  $\mathcal{O}(\eta_q \log \eta_q)$  [31]. For the GLDPC code ensemble, the density transfer function  $f_C(\cdot)$  needs to be obtained numerically [24]. Suppose the constituent generalized CNs are decoded by applying the BCJR algorithm to their respective minimal canonical trellis. If we use  $\eta_m$  Monte Carlo points to estimate  $f_C(\cdot)$ , the complexity of estimating it will be of the order  $\mathcal{O}(\eta_m 2^{\eta_c})$ , since the complexity of BCJR algorithm is exponential in the number of states [32], [33] and decoding is done for each Monte Carlo point. For GLDPC codes,  $f_V(\cdot) = \lambda(\cdot)$  and hence the overall complexity of the operation  $c_{BICM(h)} \star f_V(f_C(a))$  will be  $\mathcal{O}(\eta_m 2^{\eta_c} + \eta_q \log \eta_q)$ . For DGLDPC codes, both  $f_V(\cdot)$  and  $f_C(\cdot)$  need to be estimated numerically [25] and hence the complexity of the operation  $c_{BICM(h)} \star f_V(f_C(a))$  will be  $\mathcal{O}(\eta_m (2^{\eta_c} + 2^{\eta_v}) + \eta_q \log \eta_q)$ .

We now find the complexity of the operation  $\Gamma^V(\Gamma^C(I_{E_v}), h)$ . Let us first focus on the operation  $\Gamma^C(I_{E_v})$ . While for LDPC( $\lambda, \rho$ ) ensemble, a closed form approximation for  $\Gamma^C(\cdot)$  is available (Eq. (9)), for GDLPC/DGLDPC codes it is obtained numerically. Even though this numerical computation would require  $\eta_m$  Monte Carlo points, on contrary to  $f_C(\cdot)$ , one can precompute the function  $\Gamma^C(\cdot)$  and store it *a priori* for all possible values of  $I_{E_v} \in [0, 1]$  in the form of a lookup table (or consider polynomial approximation for it). Further,  $\Gamma^C(\cdot)$  needs to be computed once and can be done before applying algorithm of [2]. On the other hand,  $f_C(a)$  is a density transfer function and since  $a$  can potentially be any arbitrary density with the support set  $\mathbb{R}$ , is not feasible to store it *a priori*. For each density  $a$  that is obtained in an intermittent step of algorithm of [2], one needs to find  $f_C(a)$  every time using Monte Carlo simulations. Similar to direct computations  $I_{E_v}$  can also be arbitrary, however it is important to note that  $I_{E_v}$  will take any arbitrary value in the interval  $[0, 1]$  (as opposed to arbitrary density over  $\mathbb{R}$ ). Since  $\Gamma^C(\cdot)$  is stored *a priori*, for any intermittent  $I_{E_v} \in [0, 1]$ , the computation of  $\Gamma^C(I_{E_v})$  can be performed by lookup table (or via polynomial evaluation). Hence the complexity of  $\Gamma^C(I_{E_v})$  is  $\mathcal{O}(1)$ . Similarly the complexity of  $\Gamma^V(\cdot, \cdot)$  is  $\mathcal{O}(1)$ , leading to  $\mathcal{O}(1)$  complexity of  $\Gamma^V(\Gamma^C(I_{E_v}), h)$ .

Observe that for direct computations, we need to include the cost of computing density transfer functions, since one needs to numerically compute these functions for every new

density that is obtained in algorithm of [2]. On contrary, in our method we don't need to numerically compute MI transfer functions for every new value of MI (since prior storage is possible) and hence we don't need to include the cost of computing the MI transfer functions in complexity analysis. ■

In Proposition 1,  $\eta_q$  and  $\eta_m$  are typically chosen to be large integers and hence direct computation of the FP density pair is considerably complex that our simplified method. Complexity arguments similar to Proposition 1 can be derived for SC-TC and we skip the details.

**Proposition 2.** *For the given integers  $\eta_q$  and  $l$ , suppose we divide the  $\mathbb{R}^l$  into  $\eta_q^l$  subintervals. Suppose we use  $\eta_m$  number of Monte Carlo points to numerically estimate any quantity involved towards the computation of the GEXIT function. Then for a given FP density pair, the complexity of evaluating the GEXIT function over binary-input and non-binary input AWGN channel is:*

Code ensemble	Complexity with direct computation	Complexity with our simplifications
BAWGN	$\mathcal{O}(\eta_q^2)$	$\mathcal{O}(1)$
non-binary complex-input AWGN	$\mathcal{O}(\eta_m \eta_q^{ \mathbb{X} +2})$	$\mathcal{O}(\eta_m)$

*Proof:* Given the FP densities  $a$  and  $c_{BICM(h)}$ , the EBP-GEXIT function for a system with the Gray mapping can be evaluated from Eq. (7), which consists of two operations; find density  $\Lambda(f_C(a))$  and compute the expectation of the function  $l^{c_{BICM(h)}}(\cdot)$  with respect to  $\Lambda(f_C(a))$ . The complexity of finding  $\Lambda(f_C(a))$  is discussed in Proposition 1. Since the density  $\Lambda(f_C(a))$  can potentially be any arbitrary density over  $\mathbb{R}$ , in practice, this expectation is obtained via numerical integration. Towards this, we divide  $\mathbb{R}$  into  $\eta_q$  intervals and perform the integration numerically using the rectangle rule (which consists of  $\eta_q$  summations). For each of these  $\eta_q$  terms, evaluation of  $l^{c_{BICM(h)}}(\cdot)$  primarily consists of computing the division of two integrations corresponding to  $l^{c_{BAWGN(h)}}(\cdot)$  (see Eq. (4)). If these integrations are also computed via numerical integration (with the same parameter  $\eta_q$ ), the overall complexity of evaluating Eq. (7) would be  $\mathcal{O}(\eta_q^2)$ .

In our simplified method, firstly we provide a closed form approximation for  $l^{c_{BAWGN(h)}}(\cdot)$  (Appendix C), due to which the complexity of finding  $l^{c_{BICM(h)}}(\cdot)$  is of the order  $\mathcal{O}(1)$ . We then obtain the expectation of Eq. (7) using Eq. (11), which consists constant number of summations and hence the overall complexity of evaluating Eq. (7) is of the order  $\mathcal{O}(1)$ .

Let us now consider the direct evaluation of the GEXIT function for non-Gray mapping using Theorem 1, which involves finding  $A(h)$  and  $B(h)$ . From Eq. (17), the evaluation of  $A(h)$  consists of two steps; find the conditional density  $f_\xi(\cdot)$  for all possible  $\xi \in \mathbb{X}$  and then compute the expectation of the function  $R_2(\cdot)$  with respect to  $f_\xi(\cdot)$ . From Eq. (18),  $R_2(\cdot) = \mathbb{E}_Y[R_1(\cdot)]$  and in practice this expectation needs to be obtained via numerical integration by dividing  $\mathbb{R}^2$  into

$\eta_q \times \eta_q$  intervals. From Eq. (16), evaluation of  $R_1(\cdot)$  is  $\mathcal{O}(1)$  and hence the complexity of computing  $R_2(\cdot)$  would be of the order  $\mathcal{O}(\eta_q^2)$ . We now consider the evaluation of the multivariate density  $f_\xi(\cdot)$  with support set  $\mathbb{R}^{|\mathbb{X}|}$ . Firstly note that, this density does not have a closed form expression and needs to be obtained numerically. Suppose we divide  $\mathbb{R}^{|\mathbb{X}|}$  into  $\eta_q^{|\mathbb{X}|}$  intervals to quantize  $f_\xi(\cdot)$  and obtain the quantized version of  $f_\xi(\cdot)$  by empirically generating  $\eta_m$  points. Further, to find the GEXIT function, we need to find the expectation of  $R_2(\cdot)$  with respect to  $f_\xi(\cdot)$  via numerical integration. Thus the complexity of computing  $A(h)$  would be of the order  $\mathcal{O}(\eta_m \eta_q^{|\mathbb{X}|+2})$ . Using similar arguments it can be shown that the complexity of computing  $B(h)$  is  $\mathcal{O}(\eta_q^2)$  and the overall complexity of computing the GEXIT function would be  $\mathcal{O}(\eta_m \eta_q^{|\mathbb{X}|+2})$ .

With our simplified method,  $R_2(\cdot)$  is obtained from Eq. (19), which consists of constant number of summations of order  $\mathcal{O}(1)$  and hence the overall complexity of computing  $R_2(\cdot)$  would be  $\mathcal{O}(1)$ .  $B(h)$  being a special case of  $R_2(\cdot)$ , can be obtained with complexity  $\mathcal{O}(1)$ . For finding  $A(h)$ , instead of finding the density  $f_\xi(\cdot)$ , we obtain the expectation of  $R_2(\cdot)$  numerically using the procedure given in Section IV-C (see steps towards computing  $A(h)$ ). If we use  $\eta_m$  points to find this expectation, the overall cost of computing the GEXIT function would be  $\mathcal{O}(\eta_m)$ . ■

Here we wish to point out that the direct evaluation of the GEXIT function for non-binary AWGN channel involves a multidimensional integration and the integration over dimension more than 30 is a known difficult problem [34] (which is indeed the case for modulation schemes such as 64-QAM). Our simplifications enable this evaluation numerically feasible.

## VI. SPATIAL COUPLING ANALYSIS OF SC-TC

In Sections III and IV, we provided a numerically tractable method for estimating the MAP threshold. In order to illustrate the validity of our method, it is desirable to compare the estimated MAP thresholds with the estimates obtained via spatial coupling. Towards this, we study the threshold saturation for spatially coupled SC-TC schemes<sup>2</sup>. We numerically observe that, the BP thresholds of the spatially coupled SC-TC schemes do saturate to the MAP thresholds estimated via our method (see Fig. 4-(a)-(c) and ??).

We now describe a procedure for spatial coupling of SC-TC to evaluate their BP thresholds. The proposed formalism for spatial coupling was first introduced in [9] and is in spirit analogous to [7], [35], [36]. This framework is similar to that of spatially-coupled protograph-based LDPC codes. As a result, coupling parameters such as termination method, choice of base matrices, coupling rate loss, and the so-called *wave* effect are analogous (for details refer [35]). Spatially-coupled SC-TC can be obtained by the edge spreading rule

<sup>2</sup>We focus on the spatial coupling of SC-TC with Gray mapping since for other systems the decoding of SC-TC or LDPC codes becomes doubly iterative [28]. We plan to do spatial coupling analysis of the these systems in future work.

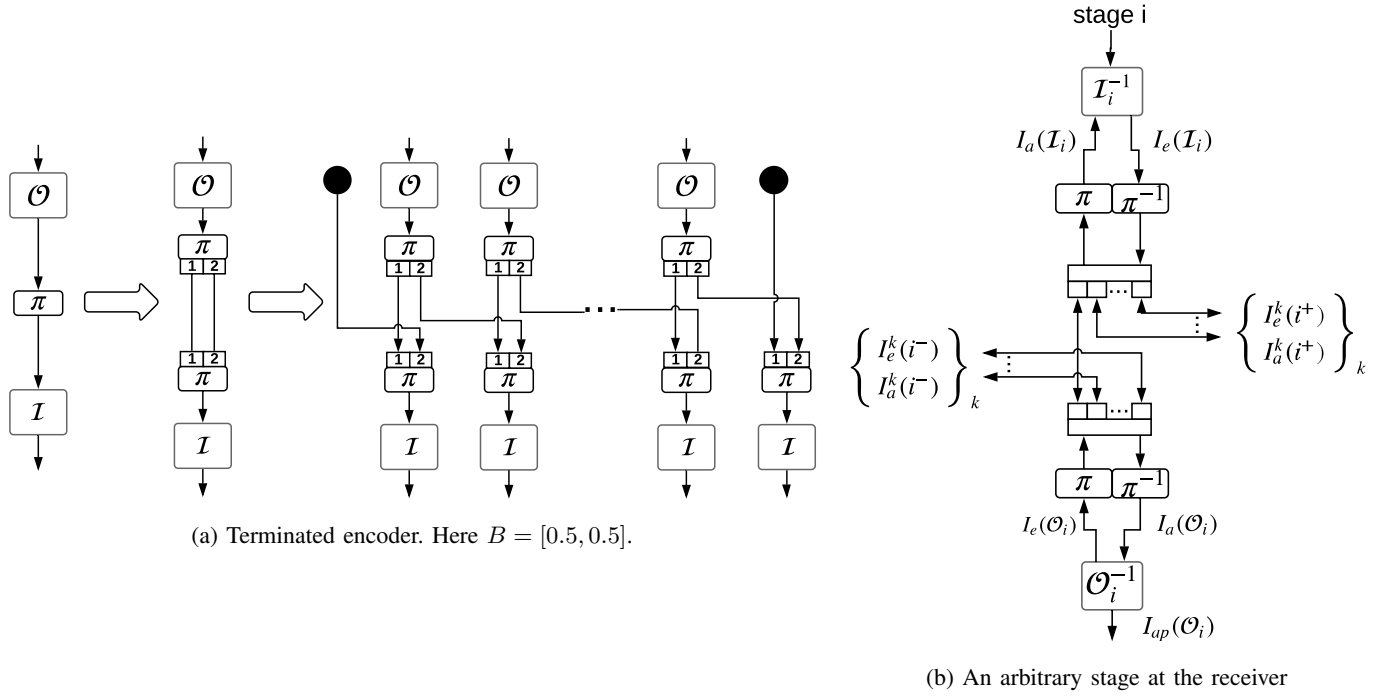


Fig. 3: Terminated SC-TC transmitter and receiver

on the factor-like graph [9]: (i) the concatenated system at the transmitter (see Fig. 1) is duplicated say  $L$  times; (ii) then the outer-code output stream  $v$  is subdivided into  $m_s + 1$  subsets; (iii) these latter are swapped between the graph duplicates by interchanging the ends of homologous subsets according to the matrix  $B := [b_0, b_1, \dots, b_{m_s}] \in [0, 1]^{m_s+1}$ , where  $b_i$  represents the  $v$  bits proportions passed from the graph copy  $t$  to  $(t + i)$ . For a better illustration of this construction, an example is illustrated in Fig. 3a. Here,  $m_s$  is called the syndrome former memory,  $L$  is the coupling length, and the coupling matrix  $B$  satisfies the equation  $\sum_{i=0}^{m_s} b_i = 1$ . It can be observed that, some bundles on the rightmost duplicates remains unconnected and there are some vacant sockets on the leftmost interleavers. This is classically addressed as follows:

- append  $m_s$  inner codes constituents  $\mathcal{J}$  at the rightmost end to connect the remaining bundles.
- "padd" with known information bits at the  $m_s$  first and the  $m_s$  last stages in order to fill all the sockets at the input of the vacant interleavers (these padding bits are depicted with black circles in Fig. 3a).

The rate of the coupled scheme can be simplified to  $R_L = R - \frac{m_s}{L+m_s}R$ . Observe that the rate loss  $\frac{m_s}{L+m_s}R$  vanishes to 0 as  $L \rightarrow +\infty$ . One can also consider other termination methods such as tail-biting [37] and code modification [38] that are proposed to mitigate this rate loss.

#### A. EXIT analysis of spatially-coupled SC-TC

For serially concatenated systems, tracking the densities associated in DE analysis become computationally difficult. In such cases, EXIT chart is a powerful tool to study the asymptotic convergence of concatenated systems under iterative decoding. First introduced in [39], its idea relies on

the fact that the density of the LLRs exchanged during the iterative decoding can be accurately modeled as consistent Gaussian. One can thus evaluate the convergence of the system by tracking the mean or the variance. We propose to express EXIT decoding transfer functions of the proposed spatially-coupled SC-TC system under BP decoding (for details refer [9]). These functions represent the MI associated with extrinsic LLR messages at the output of inner (or outer) code versus the MI associated with the *a priori* LLR messages.

In order to define the main notation, let us consider the  $i$ -th stage of the spatially-coupled factor-like graph of Fig. 3b. The corresponding notations are defined as follows:

- all variables corresponding to the stage  $i$  are referred to with the subscript  $i$ ;
- $I_a^k(i^+)$  (resp.  $I_e^k(i^+)$ ) is the *a priori* (resp. extrinsic) MI between the LLRs transmitted from  $\mathcal{O}_i^{-1}$  (resp. from  $\mathcal{J}_{i+k}^{-1}$ ) to  $\mathcal{O}_{i+k}^{-1}$  (resp. to  $\mathcal{O}_i^{-1}$ );
- Similar definitions are introduced for  $I_e^k(i^-)$  and  $I_a^k(i^-)$  with respect to the  $\mathcal{O}_i^{-1}$  and  $\mathcal{O}_{i-k}^{-1}$ .

Concerning the scheduling for spatially-coupled SC-TC decoding and similar to BP decoding of LDPC codes [1], we perform all inner updates (inner code pass) then perform all outer updates (outer code pass) according to the following the rules:

- $I_e^k(i^+) = I_e(\mathcal{J}_i).b_k$  and  $I_a(\mathcal{J}_i) = \sum I_a^k(i^+).b_k$
- $I_e^k(i^-) = I_e(\mathcal{O}_i).b_k$  and  $I_a(\mathcal{O}_i) = \sum I_a^k(i^-).b_k$
- The *a priori* MIs received from the added boundary nodes are equal to 1.

The BP threshold of spatially-coupled SC-TC is the lowest  $E_b/N_0$  such that  $I_{ap}(\mathcal{O}_i) \rightarrow 1, \forall i$ .

## VII. NUMERICAL RESULTS

For simulations, we consider the following families of LDPC, GLDPC, DGLDPC, and SC-TC.

- $\mathcal{S}_1$ : An outer rate 1/2 systematic recursive [5, 7] convolutional code with an inner rate 1 recursive accumulator of transfer function  $1/1 + D$  with BPSK modulation
- $\mathcal{S}_2$ : SC-TC code of scheme  $\mathcal{S}_1$  with 64-QAM Gray mapping
- $\mathcal{S}_3$ : Serially concatenated rate-1/2 systematic recursive [5, 7] codes with Gray 16-QAM
- $\mathcal{S}_4$ : SC-TC code of scheme  $\mathcal{S}_3$  with 16-QAM SP mapping
- $\mathcal{S}_5$ : (4, 8)-regular LDPC code ensemble of rate 1/2 with QPSK Gray mapping
- $\mathcal{S}_6$ : (2, 15)-regular ensemble of design rate 7/15 based on the Hamming(15, 11) component code designed in [24] with 64-QAM Natural mapping
- $\mathcal{S}_7$ : DGLDPC ensemble of rate 7/15 from [40] with BPSK modulation. Suppose generator matrices  $G_1$  and  $G_2$  are  $G_1 = \begin{bmatrix} 1 & 0 & 0 & 1 & 1 & 0 \\ 0 & 1 & 0 & 0 & 1 & 1 \\ 0 & 0 & 1 & 1 & 0 & 1 \end{bmatrix}$ ,  $G_2 = \begin{bmatrix} 1 & 1 & 1 & 0 & 0 & 0 \\ 0 & 1 & 1 & 1 & 0 & 0 \\ 0 & 0 & 1 & 1 & 1 & 0 \\ 0 & 0 & 0 & 1 & 1 & 1 \end{bmatrix}$ . All VNs have degree 6 and correspond to codes  $G_1$  (1% of all nodes),  $G_2$  (22%), repetition code (69%), and single parity check code (8%). All CNs nodes correspond to SPC(12).
- $\mathcal{S}_8$ : (3, 6)-regular LDPC code ensemble of rate 1/2 with 64-QAM Natural mapping

Note that  $\mathcal{S}_1$  to  $\mathcal{S}_4$  are SC-TC and  $\mathcal{S}_5$  to  $\mathcal{S}_8$  are LDPC codes. For  $\mathcal{S}_4$ ,  $\mathcal{S}_6$  and  $\mathcal{S}_8$  we have chosen non-Gray mapping. The obtained approximate EBP-GEXIT charts of all the above mentioned schemes are provided in Fig. 4 and their respective thresholds are provided in Tables I and II. In these tables, the MAP threshold and an upper bound (U.B.) on it are estimated by applying the Maxwell construction [3] and area theorem (see Theorem 2 and [2, Theorem 5]) respectively.

In Table I, we also provide the BP threshold of spatially coupled SC-TC with Gray mapping (which should approach to the MAP threshold) to illustrate the validity of our method. For spatial coupling, we have chosen  $B = [1/2, 1/2]$  ( $m_s = 1$ ) and  $L = 200$  (see Section VI). Observe that, the BP threshold of spatially-coupled SC-TC is close to the MAP threshold estimated from the EBP-GEXIT chart. The small difference between the two estimates might be due to various approximations involved in our method (see Remark 4). For the sake of independent interest, we also include the threshold bound given by the EXIT chart area theorem in Table-I, where the EXIT area is computed for the combined detector and inner code component [41]. Spatial-coupling of LDPC codes with Gray mapping is studied in [10]. While the BP-threshold of the spatially-coupled  $\mathcal{S}_5$  system with  $L = 64$  provided in [10] is  $E_s/N_0 = 0.54\text{dB}$  ( $h = 0.473$ ), our estimated MAP threshold is  $E_s/N_0 = 0.601\text{dB}$  ( $h = 0.4682$ ) (see Table II). Small difference in the two values might be due to various approximations involved in our method.

**Remark 4.** (Limitations of our method): Our method, being a numerical method, may suffer with respect to accuracy due to a variety of computational issues such as polynomial approximations for the EXIT charts, Gauss-Hermite procedure. Further, our method relies on the consistent Gaussian assumption. For the systems where this assumption is not good enough, analyzing its effect on the estimated MAP threshold is desirable, which we plan to do in future.  $\square$

**Remark 5.** (Limitations of estimating the MAP threshold via EBP-GEXIT chart): For serially concatenated systems with a non-Gray mapper as an inner code and a convolutional code as an outer code, it known that the BP threshold does not exist. A similar behavior is also exhibited by low-density generator-matrix (LDGM) codes. Therefore, EBP-GEXIT charts cannot be used for the MAP threshold estimation of these schemes. This is a well known problem and different methods are proposed to tackle this (e.g. see potential threshold approach of [6]). We plan to study such systems in future. Note that for the system  $\mathcal{S}_4$  studied in our work, we consider a SC-TC system with two convolutional codes as inner and outer codes respectively and a non-Gray mapping. For such SC-TC systems, the combined EXIT curve of detector and inner code is considered and the BP and MAP thresholds are well the defined in this case.  $\square$

## VIII. CONCLUSIONS AND FUTURE WORK

We studied the problem of estimating the MAP threshold for LDPC, GLDPC, DGLDPC, and SC-TC ensembles, when the transmission is over non-binary complex-input AWGN channel. We extended the existing results to obtain the GEXIT function over complex AWGN channel and provided a computationally tractable method for fast evaluation of an approximate EBP-GEXIT chart, based on the Gaussian approximation. We estimated the MAP thresholds for various systems and also illustrated the validity of our method by analyzing the threshold saturation for SC-TC system with the Gray mapping. We provided a complexity analysis comparing the computation cost of direct computation of the EBP-GEXIT chart versus our simplified method.

Since our proposed method for the computation of EBP-GEXIT charts only requires the knowledge of the constituent EXIT charts of a system, this opens up the applicability of our method to a variety of setups such as multiple-input multiple-output (MIMO) system, intersymbol interference (ISI) and Rayleigh fading channels. Extensions to other channel code families such as parallel turbo, LDGM, and multi-egde type (MET) LDPC codes is also of interest.

## ACKNOWLEDGMENTS

This work was funded by the DST-INSPIRE faculty program of Government of India and by the french national research agency (ANR) under grant ANR-17-CE25-0007 (MUSICO project). Authors would also like to acknowledge the support of Centre International de Mathematiques et Informatique de Toulouse, France.

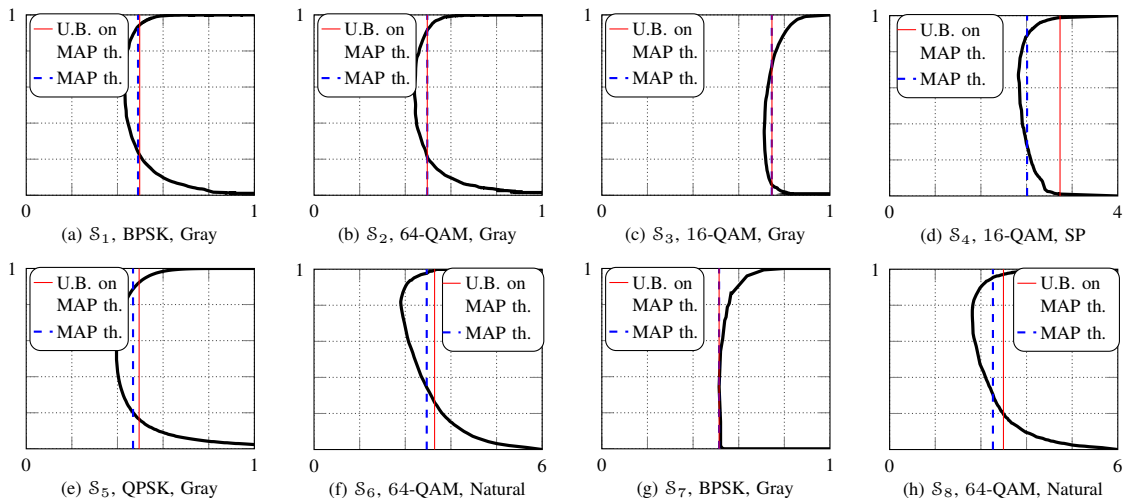


Fig. 4: EBP-GEXIT chart for systems  $\mathcal{S}_1$  to  $\mathcal{S}_8$ . On the X-axis we have the channel entropy and on the Y-axis we have the corresponding EBP-GEXIT function (black colored curve).

scheme	MAP threshold via EBP-GEXIT		BP threshold of spatially-coupled SC-TC			U.B. on MAP th. via EBP-GEXIT		EXIT area	
	$h$	$E_s/N_0$ (dB)	$h$	$E_s/N_0$ (dB)	Rate	$h$	$E_s/N_0$ (dB)	$h$	$E_s/N_0$ (dB)
$\mathcal{S}_1$	0.4893	-2.71	0.4793	-2.55	0.4975	0.4974	-2.79	0.4963	-2.74
$\mathcal{S}_2$	0.4964	9.75	0.4881	9.94	0.4975	0.4964	9.75	0.5044	9.57
$\mathcal{S}_3$	0.7241	1.20	0.7211	1.27	0.2488	0.7315	1.03	0.7433	0.73

TABLE I: Estimates of MAP thresholds for various SC-TC with Gray mapping

scheme	MAP th. via EBP-GEXIT		U.B. on MAP th. via EBP-GEXIT	
	$h$	$E_s/N_0$ (dB)	$h$	$E_s/N_0$ (dB)
$\mathcal{S}_4$	2.4096	3.2393	2.9874	0.1412
$\mathcal{S}_5$	0.4682	0.601	0.4949	0.253
$\mathcal{S}_6$	2.9641	9.1398	3.1707	8.3614
$\mathcal{S}_7$	0.514	-3.01	0.514	-3.01
$\mathcal{S}_8$	2.7164	10.0549	2.993	9.0319

TABLE II: Estimates of MAP thresholds for various SC-TC and LDPC codes

#### APPENDIX A: GEXIT FUNCTION FOR NON-BINARY COMPLEX-INPUT AWGN CHANNEL

The key idea of the proof of Theorem 1 comes from Lemma 1 of [14]. This lemma provides an expression for the  $t$ -th GEXIT function  $g_t(h)$  for non-binary real-input AWGN channel.

*Lemma 1 of [14]:* Consider  $f_{t,\xi}(\phi)$  and  $\phi_{[\xi]}$  defined in Section IV-A. Let  $p(\xi) = \mathbb{P}[X_t = \xi]$ ,  $p(y_t|\xi') = \mathbb{P}[Y_t = y_t|X_t = \xi']$ , and  $p'(y_t|\xi) = \frac{\partial}{\partial \epsilon} p(y_t|\xi)$ , where  $\epsilon = \frac{1}{2\sigma^2}$ . Then  $g_t(h)$  for  $|\mathbb{X}|$ -ary real-input AWGN channel is given by  $g_t(h) = \sum_{\xi \in \mathbb{X}} p(\xi) \int_{\phi} f_{t,\xi}(\phi) \kappa_{t,\xi}(\phi) d\phi$  where

$$\kappa_{t,\xi}(\phi) = \frac{\int_{-\infty}^{\infty} p'(y_t|\xi) \log_2 \left\{ \frac{\sum_{\xi'} \phi_{[\xi']} p(y_t|\xi')}{\phi_{[\xi]} p(y_t|\xi)} \right\} dy_t}{\int_{-\infty}^{\infty} \sum_{\xi} p(\xi) p'(y_t|\xi) \log_2 \left\{ \frac{\sum_{\xi'} p(\xi') p(y_t|\xi')}{p(\xi) p(y_t|\xi)} \right\} dy_t}.$$

It can be verified that this lemma hold true for complex-input AWGN channel as well and hence we use it to

prove our theorem. Towards this we next obtain expressions for  $p'(y_t|\xi)$  and  $p(y_t|\xi')/p(y_t|\xi)$  for complex-input AWGN channel. We first obtain an expression for  $p'(y_t|\xi)$ . Since the distribution of the noise corresponding to both real and imaginary parts is  $\mathcal{N}(0, \sigma^2)$ , the distribution of  $Y_t$  under the condition  $\xi$  is bivariate Gaussian and using this we get,

$$\begin{aligned} p'(y_t|\xi) &= \frac{\partial}{\partial \epsilon} p(y_t|\xi) = \frac{\partial}{\partial \epsilon} \frac{1}{2\pi\sigma^2} e^{-\frac{|y_t - \xi|^2}{2\sigma^2}} \\ &\stackrel{(a)}{=} \frac{\partial \sigma}{\partial \epsilon} \left( \frac{\partial}{\partial \sigma} \frac{1}{2\pi\sigma^2} e^{-\frac{|y_t - \xi|^2}{2\sigma^2}} \right) \\ &\stackrel{(b)}{=} p(y_t|\xi) (|y_t - \xi|^2 - 2\sigma^2), \end{aligned}$$

where the equality in (a) follows from the chain rule of derivative. Since  $\epsilon = \frac{1}{2\sigma^2}$ ,  $\sigma$  is a function of  $\epsilon$  and by solving the derivative we get  $\frac{\partial \sigma}{\partial \epsilon} = \sigma^3$ . Substituting this in (a) and solving the derivative we obtain (b). The fraction

$p(y_t|\xi')/p(y_t|\xi)$  is given by

$$\begin{aligned} \frac{p(y_t|\xi')}{p(y_t|\xi)} &= \left( \frac{1}{2\pi\sigma^2} e^{-\frac{|y_t-\xi'|^2}{2\sigma^2}} \right) / \left( \frac{1}{2\pi\sigma^2} e^{-\frac{|y_t-\xi|^2}{2\sigma^2}} \right) \\ &= \exp \left[ \frac{|y_t-\xi|^2 - |y_t-\xi'|^2}{2\sigma^2} \right]. \end{aligned}$$

Since  $N \gg |\mathbb{X}|$ , in presence of an ideal interleaver we can assume that the transmitted symbols are equally likely, i.e.,  $p(\xi) = 1/|\mathbb{X}| \forall \xi \in \mathbb{X}$ . Using this and substituting values of  $p'(y_t|\xi)$  and  $p(y_t|\xi')$  in Lemma 1 of [14] we get the required expression of the theorem. ■

#### APPENDIX B: PROOF OF THEOREM 2 (AREA THEOREM FOR THE SYSTEM OF FIG. 1)

The proof follows by direct application of the generalized area theorem (GAT) [2, Thm. 1]. While in [2] GAT was derived for BMS, we observe that it is also applicable for any  $|\mathbb{X}|$ -ary, complex-input memoryless channel. Suppose the channel input symbols  $\mathbf{X} = [X_1 \dots X_N]$  are transmitted via the set of parallel independent memoryless channels parameterized by  $h_1, \dots, h_N$  respectively to receive  $\mathbf{Y} = [Y_1 \dots Y_N]$ . Then from GAT we have  $dH(\mathbf{X}|\mathbf{Y}) = \sum_{t=1}^N \frac{\partial H(X_t|\mathbf{Y})}{\partial h_t} dh_t$ . If all the individual channel parameters  $h_1, \dots, h_N$  in are parameterized in a smooth way by a common parameter  $h$ , then the GEXIT function  $g(h)$  is defined in [2] as  $g(h) = \sum_{t=1}^N \frac{\partial H(X_t|\mathbf{Y})}{\partial h_t} \frac{dh_t}{dh} \Big|_h$ .

Each  $Y_t$  is a function of the  $t$ -th channel parameter  $h_t$  and can be denoted by  $Y_t(h_t)$ . Integrating  $g(h)$  from 0 to  $|\mathbb{X}|$  we get (refer to the discussion after Definition 3 of [2]),

$$\begin{aligned} \int_{\underline{h}}^{\bar{h}} g(h) &= \frac{1}{N} \left[ H(\mathbf{X}|\mathbf{Y}(|\mathbb{X}|)) - H(\mathbf{X}|\mathbf{Y}(0)) \right] \\ &\stackrel{(a)}{=} \frac{1}{N} [k - 0] \stackrel{(b)}{=} \frac{km}{n}. \end{aligned} \quad (22)$$

The equality in (a) is obtained since the entropy  $H(\mathbf{X}|\mathbf{Y}(0))$ , which is the uncertainty about  $\mathbf{X}$  in presence of zero noise, is equal to 0. Note that for the AWGN channel, noise entropy  $h = |\mathbb{X}|$  correspond to large enough (ideally infinite) noise variance such that the received  $\mathbf{Y}$  does not provide any information about the transmitted  $\mathbf{X}$ . This implies that  $H(\mathbf{X}|\mathbf{Y}(|\mathbb{X}|)) = H(\mathbf{X})$ . Since modulation scheme does not change the entropy of the transmitted codewords we have  $H(\mathbf{X}) = k$ , where  $k$  is the dimension of the code. The equality in (b) is obtained since for  $m$ -ary modulation scheme we have  $N = n/m$  (see Section II) and this completes the proof. ■

#### APPENDIX C: APPROXIMATION FOR THE GEXIT KERNEL OF BAWGN CHANNEL

For a random variable  $W \sim \mathcal{N}(2/\sigma^2, 4/\sigma^2)$  and real number  $z$ , define a function  $f(h, z)$  as

$$\begin{aligned} f(h, z) &= \mathbb{E}_W \left[ \frac{1}{1 + e^{W+z}} \right] \\ &= \int_{-\infty}^{\infty} \frac{1}{\sqrt{2\pi(4/\sigma^2)}} \frac{e^{-\frac{(w-(2/\sigma^2))^2}{8/\sigma^2}}}{1 + e^{w+z}} dw, \end{aligned}$$

where  $h = 1 - J(2/\sigma)$ . Using this in Eq. (4) we have  $l^{cBAWGN(h)}(z) = f(h, z)/f(h, z = 0)$ . The function  $f(h, z)$  can be approximated using Marquardt-Levenberg algorithm [42] as follows.

$$f(h, z) \approx \begin{cases} 1 & \text{if } z \leq L(h) \\ 1 - e^{-A_3(h)z^3 + A_2(h)z^2 + A_1(h)z + A_0(h)} & \text{if } L(h) < z < M(h) \\ 0 & \text{if } z \geq M(h) \end{cases} \quad (23)$$

where  $L(h), M(h), A_0(h), A_1(h), \dots, A_3(h)$  are approximated as polynomials of degree 10 as

$$\begin{aligned} L(h) &= -92218h^{10} + 490818h^9 - 1127499h^8 + 1463798h^7 - 1181473h^6 \\ &\quad + 614716h^5 - 207094h^4 + 44333h^3 - 5817h^2 + 467h - 38 \\ M(h) &= -33578h^{10} + 175895h^9 - 397298h^8 + 506819h^7 - 401852h^6 \\ &\quad + 205453h^5 - 68054h^4 + 14322h^3 - 1837h^2 + 136h + 1 \\ A_0(h) &= 117.76h^{10} - 610.96h^9 + 1344.72h^8 - 1634.10h^7 + 1195.44h^6 \\ &\quad - 538.70h^5 + 146.66h^4 - 22.38h^3 + 1.19h^2 - 0.33h \\ A_1(h) &= 28.89h^{10} - 155.08h^9 + 369.42h^8 - 512.31h^7 + 453.43h^6 \\ &\quad - 262.89h^5 + 98.69h^4 - 22.90h^3 + 3.18h^2 + 0.01h \\ A_2(h) &= 10.94h^{10} - 62.92h^9 + 154.13h^8 - 210.31h^7 + 175.60h^6 \\ &\quad - 93.03h^5 + 31.50h^4 - 6.78h^3 + 0.88h^2 - 0.11h \\ A_3(h) &= 0.47h^{10} - 1.58h^9 + 1.47h^8 + 0.85h^7 - 2.78h^6 \\ &\quad + 2.44h^5 - 1.11h^4 + 0.29h^3 - 0.04h^2 + 0.01h. \end{aligned}$$

#### REFERENCES

- [1] T. Richardson and R. Urbanke, *Modern Coding Theory*. Cambridge University Press, 2008.
- [2] C. Méasson, "Conservation laws for coding," *PhD thesis, EPFL, Switzerland*, 2006.
- [3] C. Méasson, A. Montanari, and R. Urbanke, "Maxwell construction: The hidden bridge between iterative and maximum a posteriori decoding," *IEEE Trans. on Info. Theory*, vol. 54, no. 12, pp. 5277–5307, Dec. 2008.
- [4] S. Kudekar, T. Richardson, and R. Urbanke, "Threshold saturation via spatial coupling: Why convolutional LDPC ensembles perform so well over the BEC," *IEEE Transactions on Information Theory*, vol. 57, no. 2, pp. 803–834, Feb. 2011.
- [5] A. Yedla, Y. Jian, P. Nguyen, and H. Pfister, "A simple proof of maxwell saturation for coupled scalar recursions," *IEEE Transactions on Information Theory*, vol. 60, no. 11, pp. 6943–6965, November 2014.
- [6] S. Kumar, A. J. Young, N. Macris, and H. D. Pfister, "Threshold saturation for spatially coupled LDPC and LDGM codes on BMS channels," *IEEE Trans. on Inf. Theory*, vol. 60, no. 12, pp. 7389–7415, 2014.
- [7] S. Moloudi, M. Lentmaier, and A. G. i Amat, "Spatially coupled turbo-like codes," *IEEE Trans. on Info. Theory*, vol. 63, no. 10, pp. 6199–6215, Oct 2017.
- [8] S. Moloudi, M. Lentmaier, and A. Graell i Amat, "Spatially coupled turbo-like codes: A new trade-off between waterfall and error floor," *IEEE Transactions on Communications*, vol. 67, no. 5, pp. 3144–3123, 2019.
- [9] T. Benaddi, C. Poulliat, and R. Tajan, "A general framework and optimization for spatially-coupled serially concatenated systems," in *Proc. of IEEE GLOBECOM*, Singapore, December 2017, pp. 1–6.
- [10] A. Yedla, M. El-Khamy, J. Lee, and I. Kang, "Performance of spatially-coupled LDPC codes and threshold saturation over BICM channels," *arXiv preprint arXiv:1303.0296[cs.IT]*, 2013.
- [11] C. Méasson, A. Montanari, T. Richardson, and R. Urbanke, "The generalized area theorem and some of its consequences," *IEEE Trans. on Info. Theory*, vol. 55, no. 11, pp. 4793–4821, Nov. 2009.
- [12] A. Yardi, I. Andriyanova, and C. Poulliat, "EBP-GEXIT charts over the binary-input AWGN channel for generalized and doubly-generalized LDPC codes," in *Proc. of IEEE ISIT*, Vail, Colorado, USA, June 2018, pp. 496–500.
- [13] T. Benaddi, A. Yardi, C. Poulliat, and I. Andriyanova, "Estimating the maximum a posteriori threshold for serially concatenated turbo codes," in *Proc. of IEEE ISIT*, Paris, France, July 2019, pp. 1347–1351.

- [14] P. Nguyen, A. Yedla, and H. P. adn K. Narayanan, "Threshold saturation of spatially-coupled codes on intersymbol-interference channels," in *Proceedings of IEEE ICC*, Ottawa, Canada, June 2012, pp. 2181–2186.
- [15] W. Ryan and S. Lin, *Channel codes: classical and modern*. Cambridge University Press, 2009.
- [16] A. G. i Fàbregas, A. Martinez, and G. Caire, "Bit-interleaved coded modulation," *Foundations and Trends in Communications and Information Theory*, vol. 5, no. 1-2, pp. 1–153, 2008.
- [17] A. Ashikmin, G. Kramer, and S. ten Brink, "Extrinsic information transfer functions: Model and erasure channel properties," *IEEE Trans. on Info. Theory*, vol. 50, no. 11, pp. 2657–2673, Nov. 2004.
- [18] A. Bennatan and D. Burshtein, "Design and analysis of nonbinary LDPC codes for arbitrary discrete-memoryless channels," *IEEE Transactions on Information Theory*, vol. 52, no. 2, pp. 549–583, 2006.
- [19] A. G. i Fàbregas, A. Martinez, G. Caire *et al.*, "Bit-interleaved coded modulation," *Foundations and Trends® in Communications and Information Theory*, vol. 5, no. 1-2, pp. 1–153, 2008.
- [20] A. Fàbregas, A. Martinez, and G. Caire, "Error probability of bit-interleaved coded modulation using the Gaussian approximation," in *Proc. of Conference on Information Science and Systems*, New Jersey, USA, March 2004.
- [21] L. Szczeciński and M. Benjillali, "Probability density functions of logarithmic likelihood ratios in phase shift keying BICM," in *Proceedings of IEEE GLOBECOM*, San Francisco, USA, November 2006, pp. 1–6.
- [22] M. Benjillali, L. Szczeciński, and S. Aïssa, "Probability density functions of logarithmic likelihood ratios in rectangular QAM," in *Proceedings of 23rd Biennial Symposium on Communications*, 2006.
- [23] *IEEE 802.16m Evaluation Methodology Document*. IEEE 802.16 Broadband Wireless Access Working Group, 2008.
- [24] G. Liva, W. Ryan, and M. Chiani, "Quasi-cyclic generalized LDPC codes with low error floors," *IEEE Transactions on Communications*, vol. 56, no. 1, pp. 49–57, January 2008.
- [25] Y. Wang and M. Fossorier, "Doubly generalized LDPC codes," in *Proceedings of IEEE International Symposium on Information Theory*, Seattle, WA, USA, July 2006, pp. 669–673.
- [26] S. Chung, T. Richardson, and R. Urbanke, "Analysis of sum-product decoding of LDPC codes using a Gaussian approximation," *IEEE Transactions on Information Theory*, vol. 47, no. 2, pp. 657–670, Feb. 2001.
- [27] M. Abramowitz and I. Stegun, *Handbook of Mathematical Functions*. New York, USA: Dover, 1970.
- [28] S. ten Brink and G. Kramer, "Design of repeat-accumulate codes for iterative detection and decoding," *IEEE Transactions on Signal Processing*, vol. 51, no. 11, pp. 2764–2772, 2003.
- [29] S. ten Brink, G. Kramer, and A. Ashikmin, "Design of low-density parity-check codes for modulation and detection," *IEEE Transactions on Communications*, vol. 52, no. 4, pp. 670–678, April 2004.
- [30] P. Jäckel, "A note on multivariate gauss-hermite quadrature," *Oxford University, Technical Report*, May, 2005.
- [31] A. Oppenheim, R. Schaffer, and J. Buck, *Discrete-time signal processing*, 2nd ed. New Jersey, USA: Prentice Hall, 1998.
- [32] L. Bahl, J. Cocke, and F. Jelinek and J. Raviv, "Optimal decoding of linear codes for minimizing symbol error rate," *IEEE Transactions on Information Theory*, vol. 20, no. 2, pp. 284–287, 1974.
- [33] R. McEliece, "On the BCJR trellis for linear block codes," *IEEE Trans. on Info. Theory*, vol. 42, pp. 1072–1092, 1996.
- [34] R. Cools, "Advances in multidimensional integration," *Jrnl. of Computational and App. Maths.*, vol. 149, pp. 1–12, 2002.
- [35] D. Costello, M. Lentmaier, and D. Mitchell, "New perspectives on braided convolutional codes," in *Proc. of ISTC*, 2016.
- [36] S. Moloudi, M. Lentmaier, and A. G. i Amat, "Spatially coupled turbo codes," in *Proc. of IEEE ISTC*, 2014, pp. 82–86.
- [37] S. Cammerer, V. Aref, L. Schmalen, and S. ten Brink, "Triggering wave-like convergence of tail-biting spatially coupled LDPC codes," in *Annual Conference on Information Science and Systems (CISS)*. IEEE, 2016, pp. 93–98.
- [38] K. Tazoe, K. Kasai, and K. Sakaniwa, "Efficient termination of spatially-coupled codes," in *ITW*, 2012, pp. 30–34.
- [39] S. ten Brink, "Convergence behavior of iteratively decoded parallel concatenated codes," *IEEE Trans. on Commun.*, vol. 49, no. 10, pp. 1727–1737, 2001.
- [40] Y. Wang and M. Fossorier, "EXIT chart analysis for doubly generalized LDPC codes," in *Proceedings of IEEE Globecom*, San Francisco, California, USA, November 2006, pp. 1–6.
- [41] J. Hagenauer, "The EXIT chart introduction to extrinsic information transfer in iterative processing," in *Proc. 12th European Signal Processing Conference (EUSIPCO)*, 2004, pp. 1541–1548.
- [42] W. Press, S. Teukolsky, W. Vetterling, and B. Flannery, *Numerical recipes in C*. Cambridge University Press, 1997.